JOURNAL OF THE ROYAL SOCIETY Interface

J. R. Soc. Interface (2010) **7**, 1677–1688
doi:10.1098/rsif.2010.0210
Published online 26 May 2010

Relative brain displacement and deformation during constrained mild frontal head impact

Y. Feng[1], T. M. Abney[1], R. J. Okamoto[1], R. B. Pless[3], G. M. Genin[1] and P. V. Bayly[1,2,*]

[1]*Department of Mechanical, Aerospace and Structural Engineering,* [2]*Department of Biomedical Engineering, and* [3]*Department of Computer Science and Engineering, St Louis 1 Brookings Drive, Box 1185, St Louis, MO 63130, USA*

This study describes the measurement of fields of relative displacement between the brain and the skull *in vivo* by tagged magnetic resonance imaging and digital image analysis. Motion of the brain relative to the skull occurs during normal activity, but if the head undergoes high accelerations, the resulting large and rapid deformation of neuronal and axonal tissue can lead to long-term disability or death. Mathematical modelling and computer simulation of acceleration-induced traumatic brain injury promise to illuminate the mechanisms of axonal and neuronal pathology, but numerical studies require knowledge of boundary conditions at the brain–skull interface, material properties and experimental data for validation. The current study provides a dense set of displacement measurements in the human brain during mild frontal skull impact constrained to the sagittal plane. Although head motion is dominated by translation, these data show that the brain rotates relative to the skull. For these mild events, characterized by linear decelerations near $1.5g$ ($g = 9.81\ \mathrm{m\ s^{-2}}$) and angular accelerations of 120–140 $\mathrm{rad\ s^{-2}}$, relative brain–skull displacements of 2–3 mm are typical; regions of smaller displacements reflect the tethering effects of brain–skull connections. Strain fields exhibit significant areas with maximal principal strains of 5 per cent or greater. These displacement and strain fields illuminate the skull–brain boundary conditions, and can be used to validate simulations of brain biomechanics.

Keywords: traumatic brain injury; displacement; deformation; magnetic resonance imaging; image registration

1. INTRODUCTION

Traumatic brain injury (TBI) is a complex injury associated with a broad spectrum of symptoms and disabilities. High linear and angular accelerations of the head often lead to diffuse axonal injury, which is generally believed to be responsible for many of the cognitive deficits exhibited by TBI survivors (Smith & Meaney 2000). Although the complete pathway from mechanical insult to cognitive deficit is not fully understood, rapid deformation of brain tissue is a biomechanical feature of most brain traumas. Clear understanding of brain displacement, stretch and stress resulting from head acceleration can help illuminate the pathology of TBI and aid in the development of preventive and therapeutic strategies.

The pattern of brain motion relative to the skull has been a focus of research for decades. Various biomechanical computer models, mostly developed using finite-element methods (e.g. Zhang *et al.* 2004) are aimed at predicting displacement and deformation of brain tissue during head acceleration. The accuracy of these models is uncertain, however, because of the lack of quantitative displacement data for comparison with predictions. The first direct observation of brain motion was performed by replacing the top of a Macacus Rhesus monkey skull with a lucite calvarium and filming the motion of the brain during impact (Shelden *et al.* 1944; Pudenz & Shelden 1946). This general method was reproduced by Ommaya *et al.* (1969) and Gosch *et al.* (1969). These experiments confirmed that the brain displaces relative to the skull, and provided qualitative insight into the deformation at the brain surface. However, the transparent replacement materials provide different boundary conditions from the intact skull, and the skull and brain of the animal itself differ significantly from the corresponding human anatomy.

The flash X-ray technique has been used by several investigators to obtain quantitative measurements of internal brain displacement in dogs (Hodgson *et al.* 1966), in primates (Shatsky *et al.* 1974) and in human

*Author for correspondence (pvb@me.wustl.edu).

Electronic supplementary material is available at http://dx.doi.org/10.1098/rsif.2010.0210 or via http://rsif.royalsocietypublishing.org.

Received 8 April 2010
Accepted 5 May 2010

cadavers (Stalnaker *et al.* 1977). During the impact or acceleration, images of lead particles embedded in the brain of the subject were obtained with high temporal resolution by fast X-ray methods. The density differences between the particles and the brain itself probably affect the displacement field. The imaging technique was improved by the use of a high-speed biplanar X-ray system to image the motion of a small number of neutral-density particles in the cadaver brain during high accelerations (Hardy *et al.* 2001). In these studies, the magnitude of the relative displacement of the brain was approximately 5 mm at the locations of the particles. In a more recent analysis of this dataset, the relative motion was separated into rigid-body displacement and deformation (Zou *et al.* 2007*a*). These two studies provide quantitative traces of human brain displacement during head impact; the major shortcomings are that the data are spatially very sparse, and that the cadaveric brain is quite different from the intact, living brain.

Magnetic resonance imaging (MRI) provides an alternative approach to investigating brain displacement. A tagged MRI protocol was performed to estimate Lagrangian strains in the human brain *in vivo* during occipital impact (Bayly *et al.* 2005) and during angular acceleration (Sabet *et al.* 2008). In these studies, although strain was estimated from the absolute displacement field, the motion of the skull was not isolated, so that relative displacement between the brain and the skull was not obtained. Displacements of the pons region of the brain under neck flexion have also been quantified using MRI techniques (Ji & Margulies 2007); however, these data correspond to quasi-static loading.

A number of mathematical models of TBI biomechanics have been developed (Zhang *et al.* 2001; Kleiven & Hardy 2002; Kimpara *et al.* 2006; Cloots *et al.* 2008; Raul *et al.* 2008; Ivancevic 2009). These models use the best available measurements of brain tissue properties and estimates of the interface conditions between the brain and the skull. However, validation of such models has suffered from the relative paucity of high-resolution experimental measurements of acceleration-induced brain displacement and deformation.

The present study extends our previous work (Bayly *et al.* 2005; Sabet *et al.* 2008) by focusing on the brain displacement with respect to the skull. A landmark point-based image registration method was applied to characterize the rigid-body motion of the skull. Material points in the brain were tracked by 'harmonic phase' (HARP) analysis of tagged MR images. The relative displacement of brain tissue with respect to the skull was acquired by expressing the brain displacements in a skull-fixed coordinate system. These results will be valuable for validation of computer models of brain biomechanics and for clarifying the role of the brain's suspension in TBI.

2. MATERIAL AND METHODS

2.1. MRI procedures

Data were obtained from three male human volunteers (age 23–44 years). Each subject lay prone on the bed of a clinical MR scanner (Siemens Sonata 1.5 T; Siemens, Munich, Germany). The head of the subject was suspended by a broad elastic strap that covered the forehead, and by a soft chin strap, both of which were attached to a rigid fibreglass frame (figure 1). This frame, which fits inside the standard Siemens head coil, rotated about a pivot that allowed constrained motion in the anterior–posterior direction. Upon release of a latch, the frame would drop approximately 2 cm and hit a rubber stop. The head would be decelerated by the elastic suspension, experiencing acceleration typical of mild frontal impact. Imaging was triggered by an optical sensor that detected the release of the latch, so that image acquisition was synchronized with motion. To maximize temporal resolution, the MR image is acquired for one line of frequency domain ('k-space') at a time; the head drop was repeated once for each line of k-space. The basic experimental equipment and procedure is similar to that illustrated and described in Bayly *et al.* (2005). The study protocol was reviewed and approved by the Washington University Human Research Protection Office.

Tagged MR images were obtained in a sagittal plane of the left hemisphere of each subject (figure 2 and electronic supplementary material, video S1*a–c*) offset about 1 cm from the mid-plane of the brain. Tagging (the application of a grid pattern to the MR images) is accomplished by imposing a temporary periodic spatial modulation to the longitudinal magnetization of spin packets, accomplished non-invasively by a combination of radio frequency pulses and magnetic field gradients (Axel & Dougherty 1989). Tagging steps were incorporated into a standard fast gradient echo cine pulse sequence (FLASH2D) with repetition time TR = 5.6 ms and echo time TE = 2.9 ms. The k-space matrix was 144×384 (144 phase-encoding line and 384 readout points). Images were obtained by zero-padding the matrix to 192×384 in the Fourier domain, Fourier transforming and truncating to a 192×192 pixel matrix. The final field of view was 250×250 mm and the slice thickness was 5 mm, corresponding to a voxel size of $1.3 \times 1.3 \times 5$ mm.

For each subject, a total of 120 images was obtained, spanning the duration of the head drop; each image frame was captured every 5.6 ms. The time between the release of the latch (initiation of imaging) and impact with the stop was approximately 40–50 ms, so that the impact typically occurred between the eighth and the tenth image. For this reason, we selected the first 30 image frames for analysis. After the first 30 frames (168 ms), the head was almost stationary.

2.2. Estimation of skull motion

To describe brain motion relative to the skull, the (approximately) rigid-body motion of the skull must be estimated. This was done by registration of landmark points on the skull and on the relatively rigid anatomical features of the head. The Cartesian coordinates of 10 landmark points were manually identified by clicking at intersections of tag lines on the reference image (figure 3*a*) and at corresponding tag line intersections

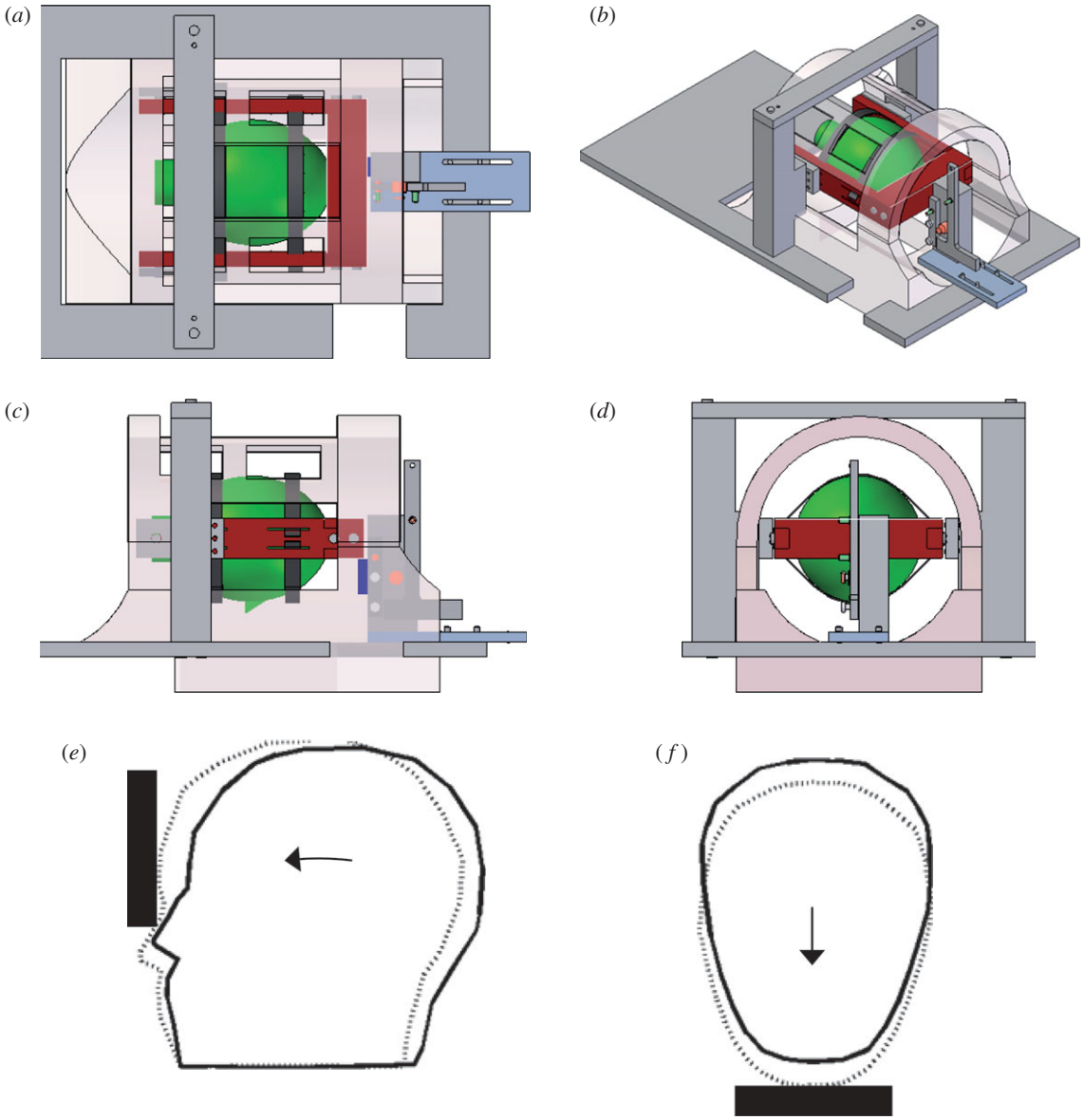

Figure 1. (*a–d*) Digital solid model of the experimental apparatus: top, isometric, side and front views. The head (green) is suspended by elastic straps (black) in a fibreglass frame (red) that can rotate in the sagittal plane to produce a nodding motion of the head. The subject lifts his lead into position, then releases a latch that drops the frame approximately 2 cm onto a stop (dark blue). (*e*,*f*) The subject's forehead is restrained by the elastic suspension to produce a mild deceleration similar to frontal impact.

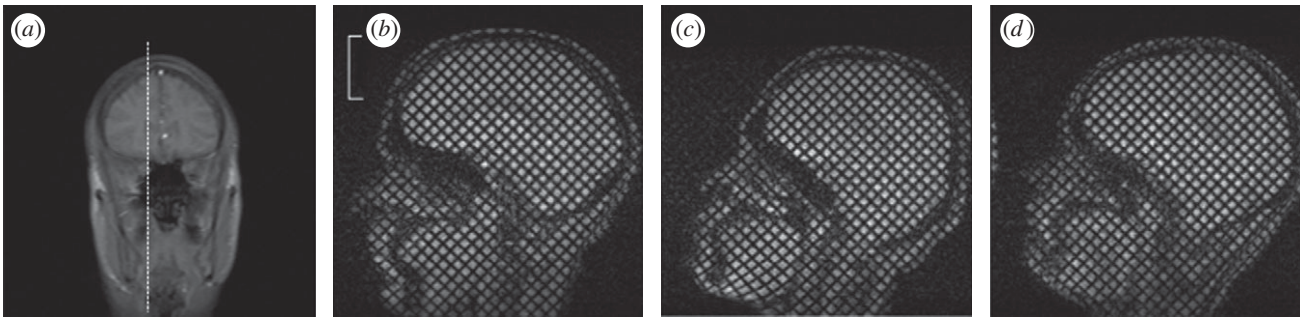

Figure 2. (*a*) Scout MR image showing the sagittal plane used for subsequent dynamic tagged imaging. (*b–d*) The (undeformed) reference grid pattern obtained by tagged MRI of this sagittal image plane in (*b*) subject S1, (*c*) subject S2 and (*d*) subject S3. (*b*) Scale bar, 5 cm.

on subsequent (deformed) images (figure 3*b*). Displacement vectors between the landmark points in the reference image and the corresponding points in each deformed image are obtained. The origin of a skull-fixed coordinate system was defined in the reference image, near the foramen magnum. We sought the rotation about the axis normal to the image plane passing through this point, combined with translation,

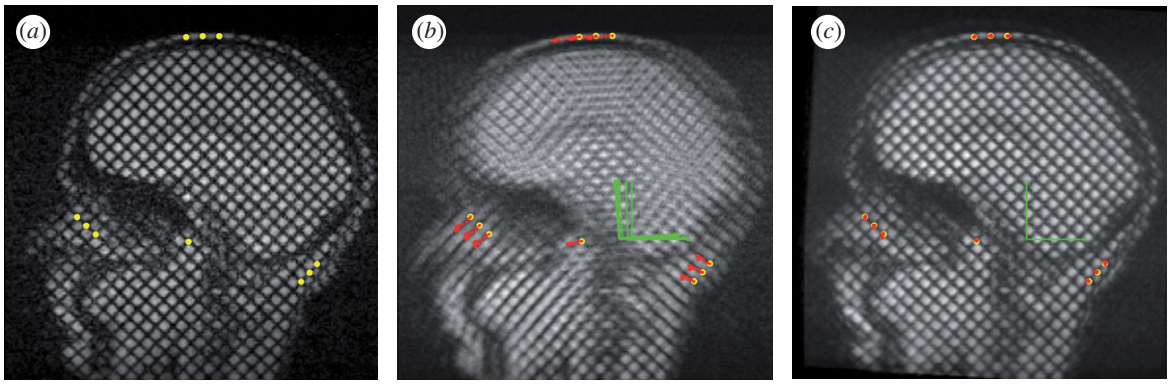

Figure 3. Quantification of the rigid-body kinematics of the head by registration of landmark points. (*a*) Ten landmark points (yellow) located at tag line intersections on extracranial tissue. (*b*) Trajectories of landmark points during head motion are shown (in red) on a composite image formed from the sum of 12 successive images (2–13). (*c*) The same set of landmark points (red) are shown *after registration* on a composite image formed from the sum of 12 successive *registered* images. Registration was performed by finding the translation and rotation of a reference frame fixed to the skull, which minimized the sum of the squared displacements of all 10 points.

which would bring the landmark points in the images of the rotated head into alignment with the landmark points in the reference image. For each image, a minimization algorithm (Nelder–Mead unconstrained nonlinear minimization) implemented in Matlab (*fminsearch*; The Mathworks, Natick, MA, USA) was used to find the three parameters (rotation, *x*-translation, *y*-translation) that minimized the sum of the squared displacements of the 10 landmark points. (An elegant alternative approach, which produces an analytical solution to the minimization problem, is described in Zou *et al.* (2007*a*)). The parameters obtained for each image were used as initial guesses for registration of the subsequent image. The registration method and results are illustrated in figure 3*b*,*c* and electronic supplementary material, video S2*a*,*b*. In figure 3*b*, the displaced landmark points are plotted on a composite image obtained by summing the images of the displaced head. In figure 3*c*, the rotation and translation are applied to each set of landmark points, and each greyscale image (using the Matlab function *imtransform*). The composite image obtained from the sum of the registered skull images and the registered landmark points are shown in figure 3*c*.

2.3. Estimation of displacement and deformation in brain tissue

The intersections of tagged lines were tracked by identifying contours of HARP (Osman *et al.* 2000). The intersection points of the brain in its deformed configuration were obtained from each MR image, and transformed so that they were expressed with respect to the skull-fixed coordinate system. The intersection points in the reference configuration were also obtained from the first MR image (before the drop). The relative displacement field was obtained from the differences in locations of intersection points in the deformed and reference configurations.

The strain distribution was obtained from the HARP intersection points via the algorithm presented in Bayly *et al.* (2005). Briefly, the Delaunay method was used to generate a triangular mesh from intersection points in the reference configuration and in the deformed configuration. For each triangle, the sides of the triangle in the reference configuration are the vectors $\mathbf{DX}_n$ ($n = 1, 2, 3$) and in the deformed configuration, the sides are $\mathbf{dx}_n$. The two-dimensional deformation gradient tensor $\mathbf{F}$ relates corresponding sides in the reference and deformed configurations

$$\mathbf{dx}_n = \mathbf{F} \cdot \mathbf{DX}_n. \tag{2.1}$$

The eigenvalues (λ_1, λ_2) of the deformation gradient tensor are the principal stretch ratios; if an infinitesimal circle is mapped by $\mathbf{F}$ from the reference to the deformed configuration, the stretch ratios are the ratios of the major and minor axes of the ellipse to the radius of the undeformed circle. The Lagrangian strain tensor $\mathbf{E}$ can be also obtained using the definition

$$\mathbf{E} = \frac{1}{2}(\mathbf{F}^T\mathbf{F} - \mathbf{I}). \tag{2.2}$$

Lagrangian strain is unaffected by rigid-body rotations.

3. RESULTS

3.1. Displacements

Estimates of skull motion in all three subjects are shown in figure 4. The peak translational acceleration magnitudes of the skull origin for the three subjects were 14.3–16.3 m s^{-2}. Peak angular accelerations for the subjects' skulls varied from 124 to 143 rad s^{-2} and occurred fairly uniformly at about 40 ms after latch release (table 1). Displacement vector fields and displacement magnitude fields for subject S1 (figure 5) show a spatially varying, dynamic pattern of relative brain displacement. For subject S1, at 39 ms (just before peak deceleration), most displacement vectors are pointing forward (anterior) but large regions have very small displacement values. From 39 to 50 ms, as the skull decelerates, the anterior components of displacement increase as the brain pitches forward relative to the

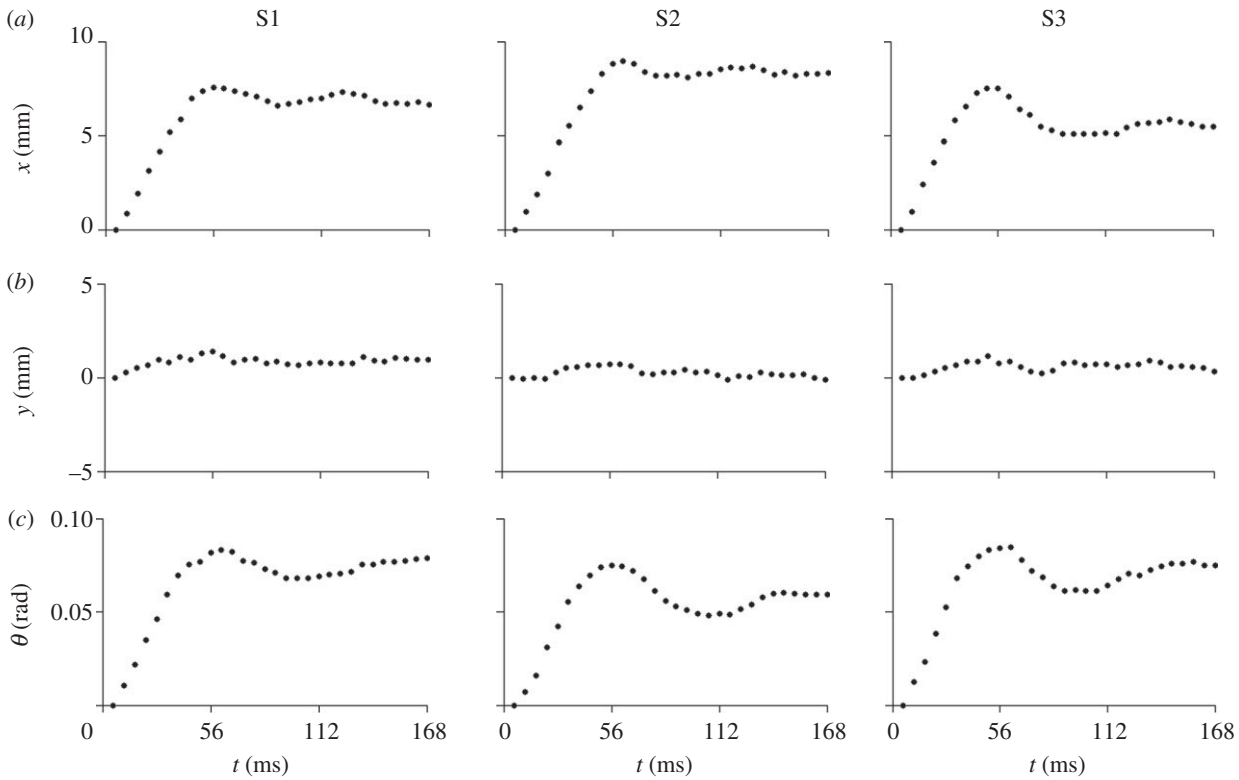

Figure 4. Estimated rigid-body motion of the skull in the first 30 images after the head drop is triggered. (*a*) Displacement of the skull origin (figure 3) in the image *x*-direction (anterior–posterior, or vertical direction for the prone subject) for subject S1, subject S2 and subject S3. (*b*) Displacement of the skull origin in the image *y*-direction (inferior–superior, or horizontal direction for the prone subject) for subject S1, subject S2 and subject S3. (*c*) Angular displacement of the skull for subject S1, subject S2 and subject S3.

Table 1. Maximum magnitude of skull linear and angular acceleration for each subject, and the corresponding time of occurrence. Linear acceleration is estimated at the centroid of the image.

	$\lvert a\rvert_{\max}$ (m s^{-2})	time (ms)	$\lvert\alpha\rvert_{\max}$ (rad s^{-2})	time (ms)
S1	14.3	44.8	131	39.2
S2	15.8	56.0	124	39.2
S3	16.3	56.0	143	39.2

skull, especially in the mid-superior cortex. Notably, near the cortical surface, the relative displacements are small; despite being surrounded by cerebrospinal fluid, the tangential motion of the surface of the brain is apparently constrained by the skull. By 56 ms, the relative displacement has begun to diminish throughout the brain. A vortex-like feature is seen in the basal central region of the field at 61.6 ms. Subsequent displacement fields (not shown) show relative displacements returning to normal values close to zero.

Figures 6 and 7 (and electronic supplementary material, video S3*a–c*) show comparisons of displacement vectors and their magnitudes in all three subjects. The maximum displacement for subject S1 is about 3.5 mm; in subject S2 about 2 mm and in subject S3 about 3 mm. The brains of the two younger subjects (S1, 23 years and S3, 30 years) exhibited more similar timing and slightly larger magnitudes than the brain of the third subject (S2, 44 years). The vortex-like feature noted above in subject S1 is also seen in subjects S2 and S3, indicating that perhaps this feature is a consistent effect of the basal attachment of the brain to skull. Relative displacement was also tracked over time at specific locations (a–d in the upper-right panel, $t = 44.8$, S3, in figure 7). We examined displacements at material positions in the frontal lobe (a), parietal regions (b), cerebellum (c) and near the pituitary stalk (d). The time series are shown in figure 8. The tissue displacements in all subjects peaked slightly before 56 ms. Larger displacements were observed in the superior cortical locations than in the basal regions (consistent with the 'pitching-forward' rigid-body component of brain motion).

3.2. Deformation

To illustrate deformation, a 'strain ellipse plot' is shown for all three subjects in figure 9. The deformation gradient $\mathbf{F}$ is used to transform circles located at different positions of the undeformed brain into corresponding ellipses in the deformed configuration. The ellipses are coloured by the corresponding maximum principal stretch ratio λ_1. These deformation fields show diffuse but heterogeneous stretching throughout the brain. The highest levels of stretch and shear are seen at the cortical surface of the brain (including frontal, superior, and occipital sites) and near basal points of attachment of the brain to the skull. Significant regions of the brain exhibit maximal principal stretches of 1.05–1.07 (5–7% elongation) under the conditions of this study. In the

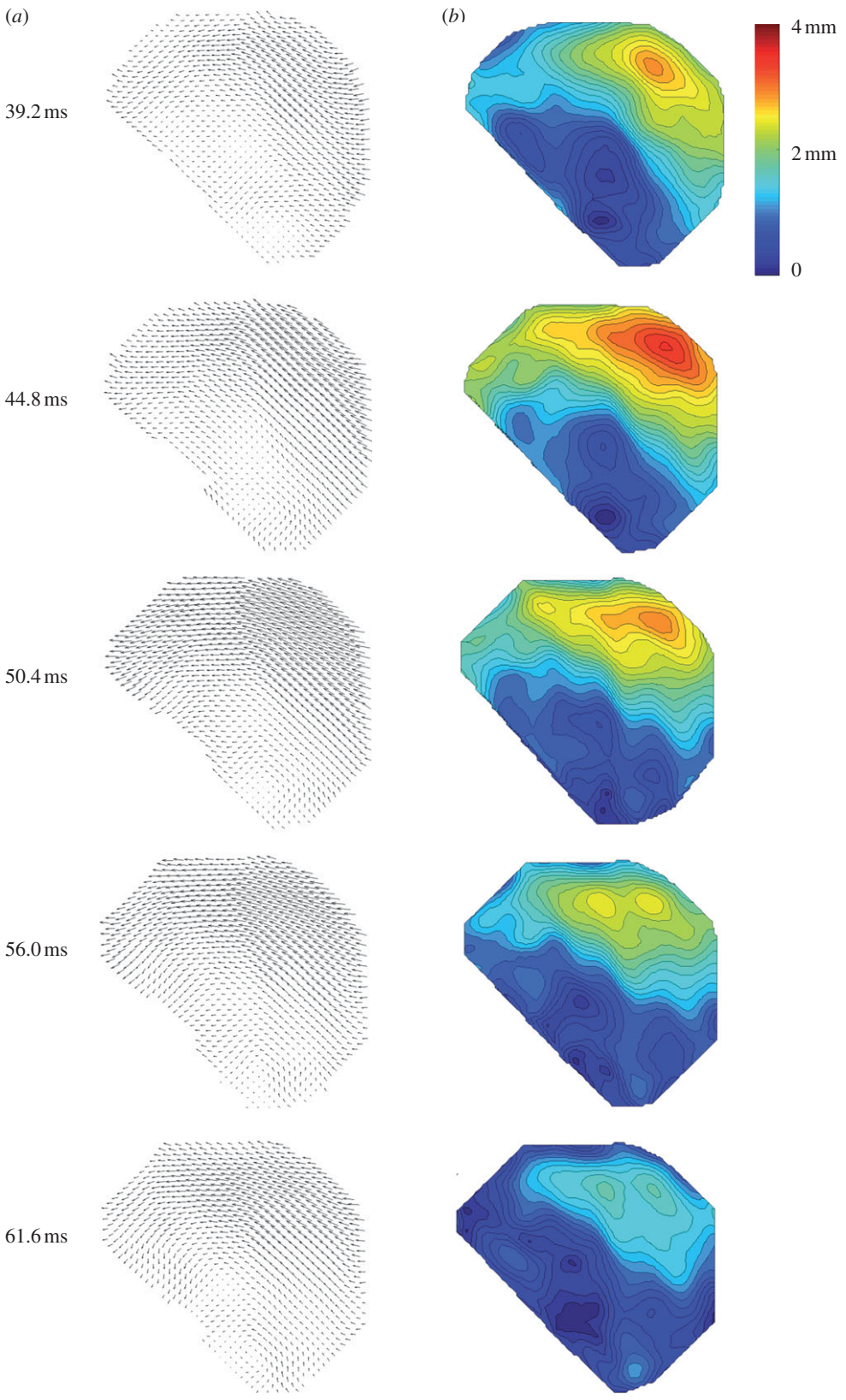

Figure 5. (*a*) Relative displacement vector field and (*b*) relative displacement magnitude field for subject S1 at $t = 39.2$ ms (image 7) after release; $t = 44.8$ ms (image 8); $t = 50.4$ ms (image 9); $t = 56.0$ ms (image 10); $t = 61.6$ ms (image 11).

Cartesian reference frame with the x-axis aligned in the anterior–posterior direction, and the y-axis aligned inferior–superior, these cortical regions are characterized by strong x–y shear deformations and vertical stretching. Time histories of the first (maximum) principal Lagrangian strain, ϵ_1, at the locations identified in figure 7, are shown in figure 10. Though the strain histories are noisier than displacement (largely because strain represents the spatial derivative of displacement), peaks near 5 per cent strain are seen

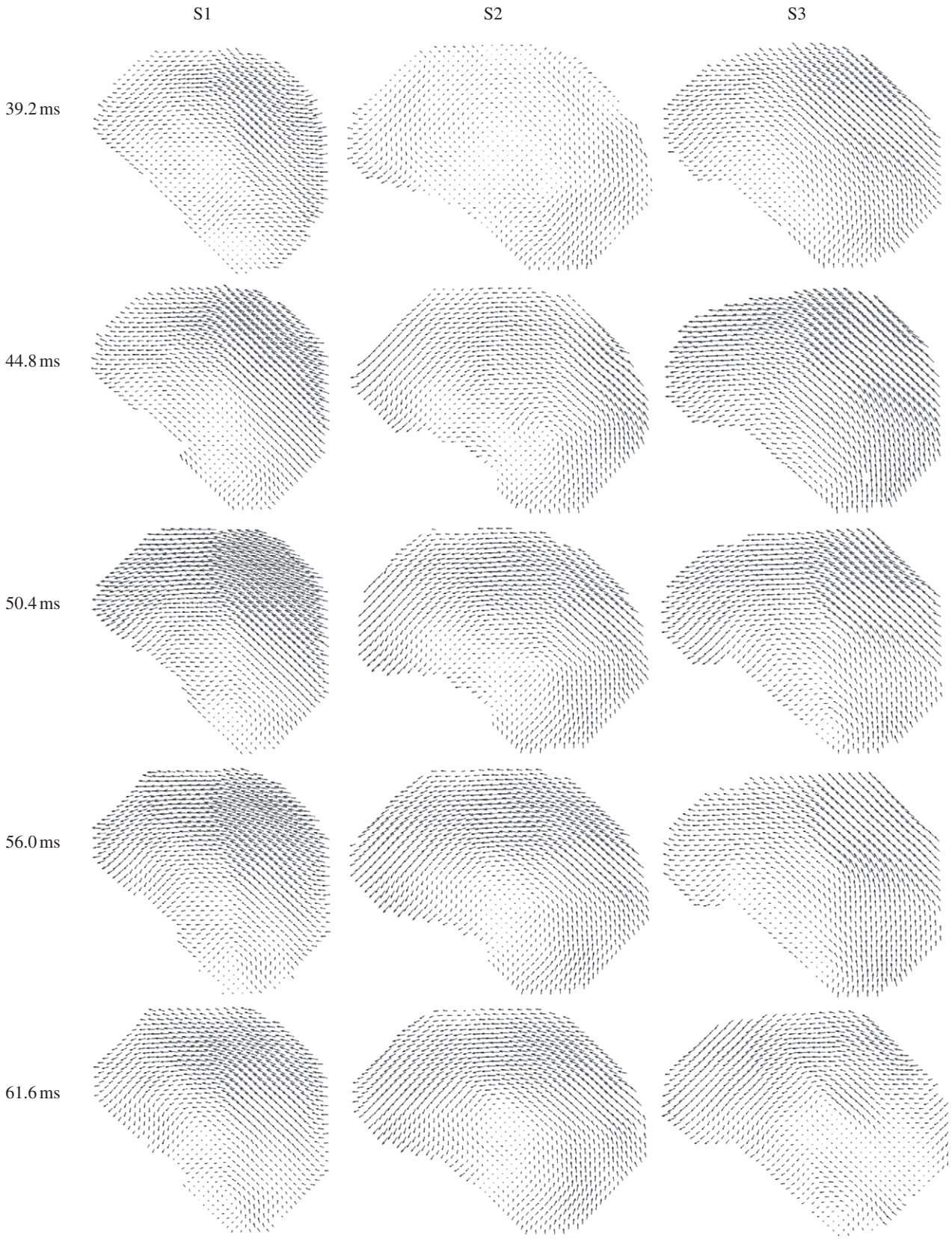

Figure 6. Relative displacement vectors, with respect to the skull, of material points in the brain in three subjects (S1, S2 and S3) at specified times after release.

consistently at locations near the superior cortical surface, around the time of peak deceleration. Strains in the inferior central region (site c) are consistently lower than strains near the superior cortical surface (sites a and b).

4. DISCUSSION

The biomechanics of TBI have been a topic of active research for decades, and computer modelling is becoming increasingly important (Zhang *et al.* 2001;

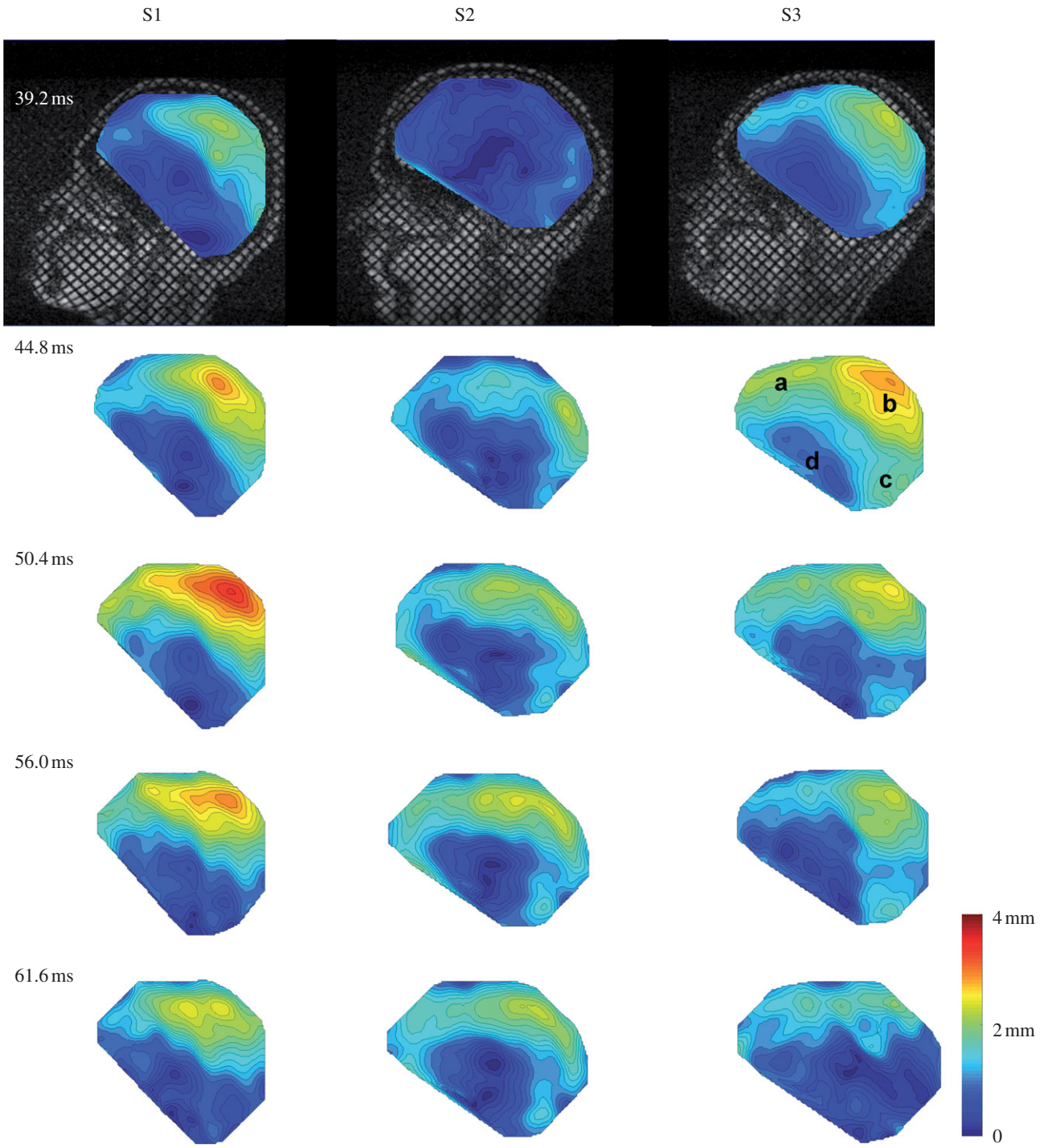

Figure 7. Relative displacement magnitudes, with respect to the skull, of material points in the brain in three subjects (S1, S2 and S3), at specific times after release, corresponding to the vector fields in figure 6. The annotations in the upper-right image (S3, $t = 44.8$) indicate the locations of points at which displacement time series are extracted and shown in figure 8.

Raul *et al.* 2008). Data showing the relative displacements in the brains of human subjects during head acceleration are useful for both the development and validation of simulations. Zhang *et al.* (2001) and several other groups have used human cadaver data from Hardy *et al.* (2001). These prior data provide useful information on the brain's response to high acceleration, but suffer from limited spatial resolution and spatial coverage, as well as from the differences between cadaveric specimens and live humans. The current study provides well-resolved fields of relative displacement in the brains of live human subjects during mild acceleration, showing the time-varying, non-uniform distribution of relative displacement in a two-dimensional sagittal plane. Oscillating patterns of displacement between the brain and the skull were found, owing to both relative rigid-body motion and deformation. The small experimental sample, which spans a relatively large age range, shows distinct individual differences in relative brain displacement under similar acceleration loading.

The patterns of displacement and deformation can be partially explained by the following scenario.

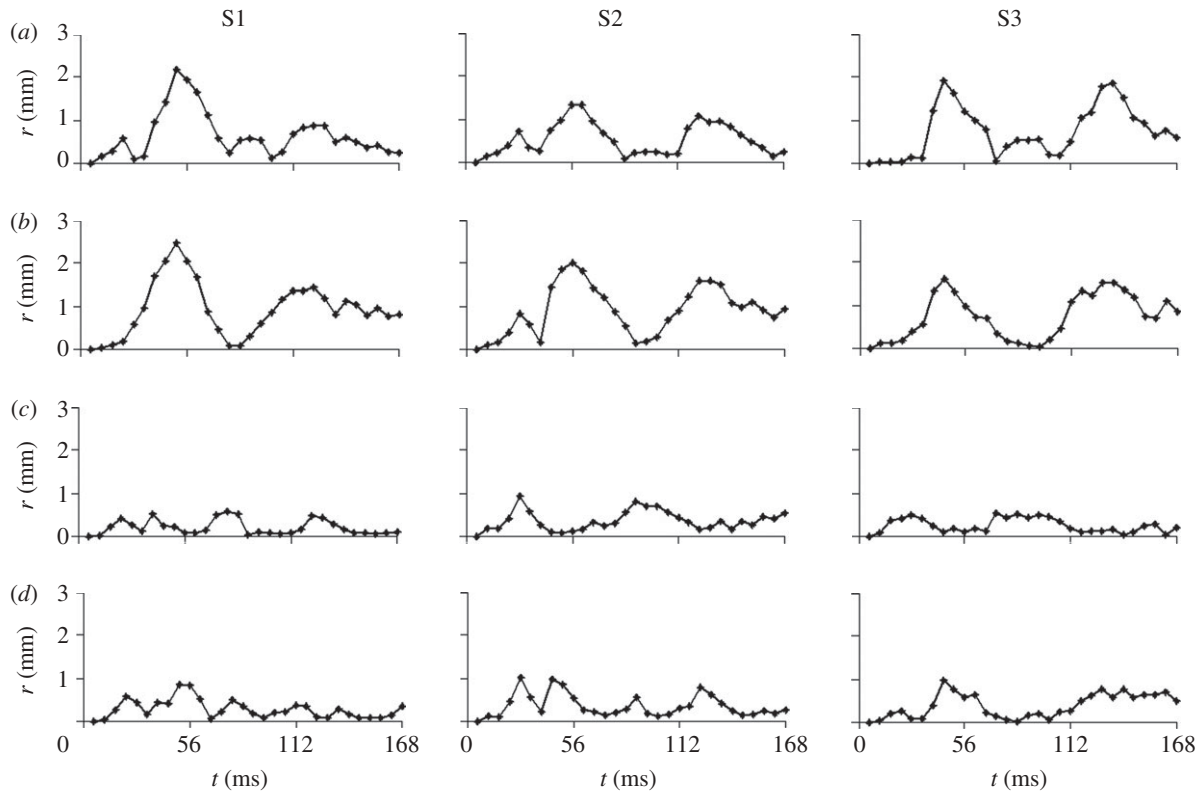

Figure 8. Time series of relative brain displacement in all three subjects at the four material locations (a, b, c and d) indicated in the upper-right panel (S3, $t = 44.8$ ms) of figure 7, for all three subjects.

Connections between the skull and the brain exist at the brain stem, and at various vascular, neural or membranous connections at the base and boundary of the brain. Very roughly, the brain can be thought of as a mass suspended by springs in a rigid container (figure 11). Impact or rapid deceleration of the container will induce oscillation of the mass, which is grossly analogous to the motion of the brain inside the skull (Zou *et al.* 2007*b*). This simplified model also illustrates why the brain has the large displacement magnitude at the boundaries and the displacement near the base is usually smaller. It appears as though the attachment of the brain to the skull is firmest at its base, so that the deceleration of the skull induces brain rotation as well as translation (Bayly *et al.* 2005; Zou *et al.* 2007*a*,*b*).

Contrary to this simple model, however, displacement in the brain does not reflect only rigid-body motion; rather the spatially and temporally varying displacement field reflects dynamic deformation (figures 5–10). A vortex-like pattern in the displacement field arises near the time of peak deceleration (figures 5 and 6). This reflects the apparent shearing deformation of soft brain tissue. The occurrence of peak relative brain displacement around the time of maximal deceleration is consistent with simple physical models and with observations from previous studies of the anaesthetized monkey brain (Shatsky *et al.* 1974). Deformation is characterized by spatial gradients of the displacement field. Here, we illustrate deformation by strain ellipse plots (figure 9), which also exhibit oscillatory (figure 10), spatially varying patterns. In all the subjects, at different times, large stretches occur near the superior surface of the cortex, in basal frontal regions and at the back of the occipital lobe. These features all appear to show the brain pulling away from attachment points, rather than compressing owing to contact with the walls of the skull. Tethering at the base of the brain is likely to contribute to these strain patterns. Stiff anatomical features in this region that connect the brain to the skull and penetrate the soft brain parenchyma include bony prominences, internal carotid arteries, the optic nerves, the olfactory tracts, the oculomotor nerves and the pituitary stalk.

Our results are generally consistent with those reported by earlier investigators, such as Hodgson *et al.* (1966), Hardy *et al.* (2001) and Zou *et al.* (2007*a*). Hardy *et al.* (2001) show that the displacement–time curve in the impact direction has a sinusoidal shape for all three of their cadaveric subjects. In the work of Hardy *et al.* (2001), the peak linear accelerations and angular accelerations are at least two orders of magnitude greater than those of the current study, but the magnitude of displacement is only about 4–5 mm (approx. 50% more than our results). This may be due to (i) nonlinear effects (the brain makes contact with the walls of the skull; slack in vessels and membranes is taken up), (ii) differences between cadavers and live humans (the cadaveric brain is probably much stiffer than the live brain), and (iii) the viscoelastic stiffening of the brain and other soft tissue at high strain rates. The duration of acceleration is also longer in the current study. Zou *et al.* (2007*a*) note in their studies of neutral-density markers that relative brain–skull displacement magnitudes increased very little as skull accelerations increased from 12 to 100g (120–1000 m s^{-2}).

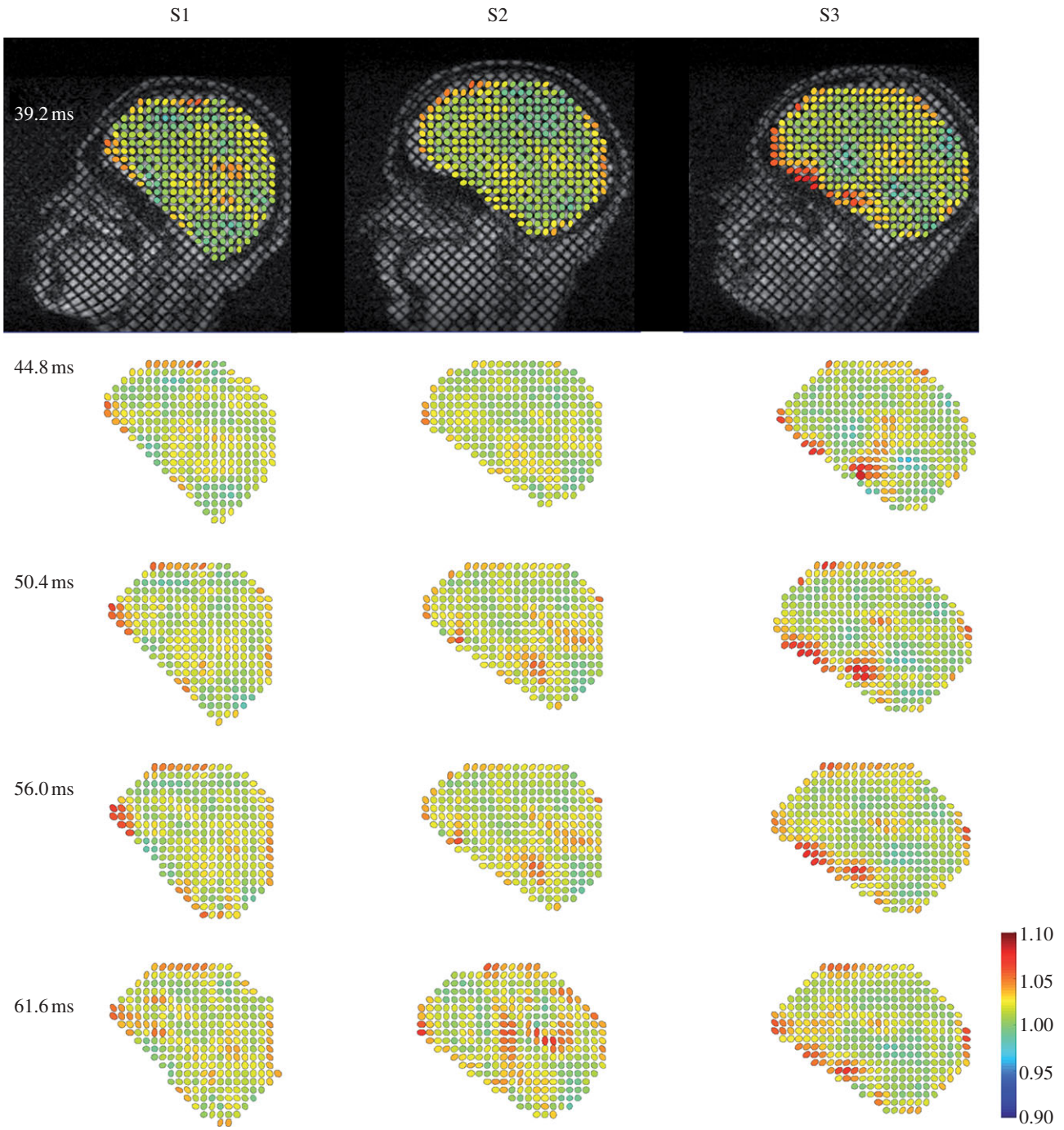

Figure 9. Strain ellipse plots for all three subjects at specified time points. Each ellipse is formed by using the deformation gradient tensor to map the undeformed circle into its corresponding elliptical deformed configuration. The centre-to-centre distance between undeformed circles is 6.5 mm and the original radius is 1.9 mm. Each deformed ellipse is coloured by its maximum principal stretch ratio λ_1 at the sampled point.

The methods of the current study are aimed at providing a comprehensive map of displacement in a two-dimensional section of the brain. This is in contrast, for example, to the complementary study of Hardy *et al.* (2001) in which displacement was obtained at only the few locations where neutral-density targets were located. However, the high accelerations used in the study of Hardy *et al.* (2001) are directly relevant to TBI; the accelerations used in the current study probe only the response to subinjury levels of acceleration. Ji & Margulies (2007) investigated the quasi-static motion of the pons inside the skull by comparing *in vivo* MR images of the undisplaced and displaced pons. The displacement field was obtained with an auto-correlation technique with resolution of the order of pixel size. The point-based registration method used in the current study proved preferable because motion artefact in MR images can confound greyscale-based registration methods. The current method can provide subpixel accuracy, given accurate manual identification of landmark points. Zou *et al.* (2007*a*) separated the relative displacement of the brain with respect to the skull into a rigid-body component and a deformation component. However,

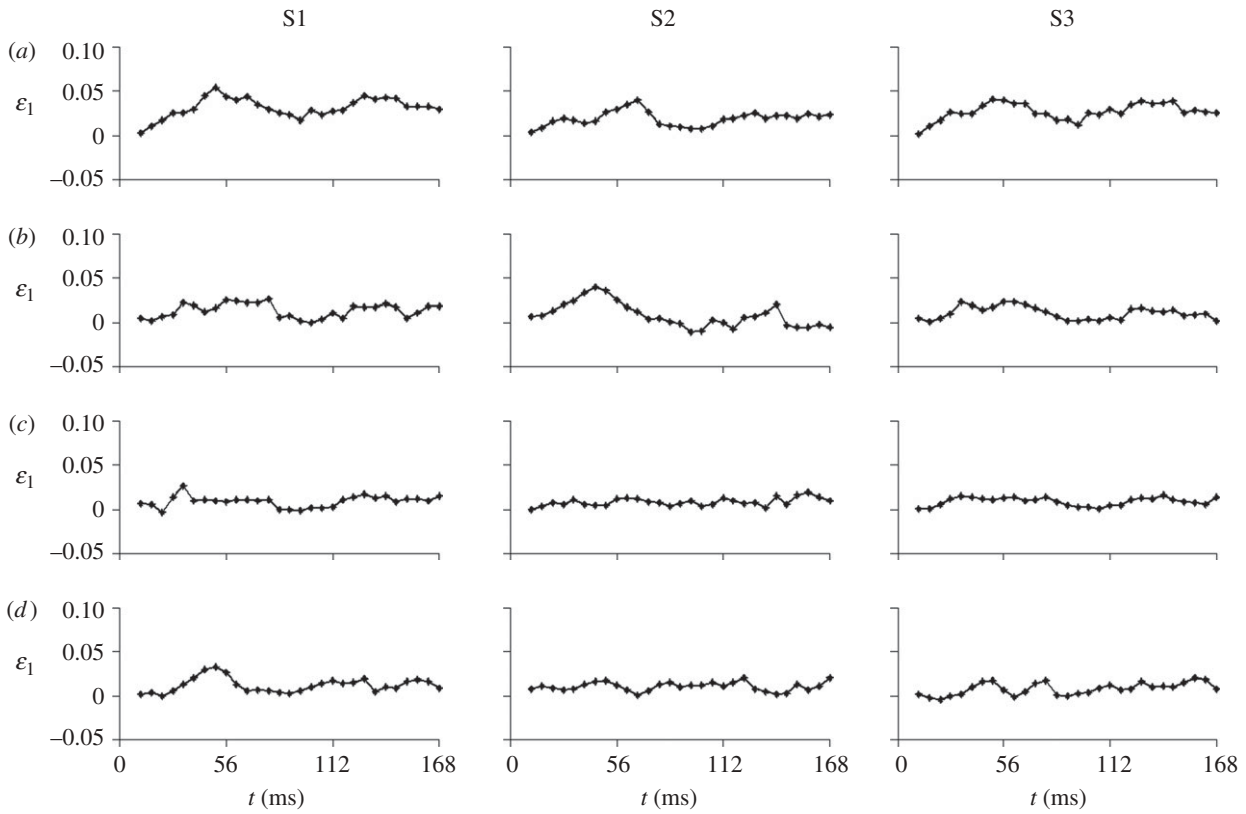

Figure 10. Time series of maximum principal strain in all three subjects estimated at the four material locations (a, b, c and d) indicated in the upper-right panel (S3, $t = 44.8$ ms) of figure 7.

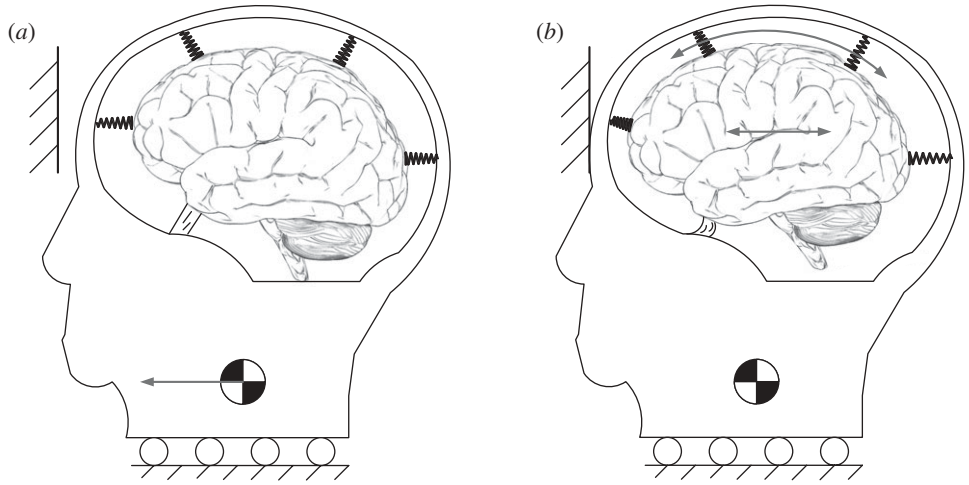

Figure 11. A highly simplified model for the gross motion of the brain in its elastic suspension. The skull is shown in pure translation. The elastic element at the base and the springs at the perimeter represent the brain's attachments to the skull. Note that linear deceleration of the skull leads to both linear and angular displacement of the brain relative to the skull.

Zou *et al.* (2007*a*) used the spatially sparse data from the study by Hardy *et al.* (2001). The current study provides complementary information: higher spatial resolution over a larger spatial domain, but at lower accelerations.

The current study is limited to motion of the brain and skull in a sagittal plane during mild decelerations approximating frontal impact. Since the deceleration is in this plane, and the plane is near the midline of the symmetric brain, out-of-plane displacements are expected to be much smaller than in-plane displacements. If volume invariance is assumed, the magnitude of out-of-plane stretching or compression can be estimated from the in-plane change in area, since the determinant, J, of the deformation gradient (the product of the principal stretches) is unity. Using this estimate, out-of-plane strains do not exceed 1 per cent in this study. However, the effects of out-of-plane motion may not be negligible. It is almost certain that anatomical features outside the image plane affect the motion of points in this plane. Such features include the falx cerebri, the tentorium, various vessels, bony prominences and membranous sheaths of major nerves. By increasing the number of imaging

planes, three-dimensional displacement fields can be constructed. However, using the current technique, this would require more repetitions of impact, which are undesirable in human subjects. Extension of this technique to an animal model would facilitate the acquisition of more complete spatial information, but would be less relevant to the problem of human brain injury. Temporal resolution in the current study is 5.6 ms, obtained by a standard 'fast, low angle' (FLASH2D) gradient echo imaging sequence. More advanced fast imaging techniques should allow increased temporal resolution in future studies. Accuracy of image registration relies on good image quality (high signal-to-noise, low blurring) and high resolution, which are competing goals of the MR pulse sequence. The current set of MR pulse sequence and sequence parameters appears to provide an appropriate compromise, which, again, may be improved by new MR sequences in future work.

In conclusion, this study provides the first comprehensive, high-resolution, quantitative data on the relative displacement of the brain with respect to the skull caused by mild frontal impact. The results can be used to validate models of brain trauma, understand mechanisms of TBI and improve the understanding of the mechanical properties of brain tissue. This approach complements both experimental studies of the cadaveric and animal brains under high accelerations, and numerical studies of injury mechanics in the human brain. Future studies will aim to continue to improve our quantitative knowledge of the kinematics of the human brain during linear and angular skull acceleration.

We gratefully acknowledge the assistance of Richard Nagel in acquisition of tagged MR images. Funding for the study was provided by the National Institutes of Health grants NS055951 and HL079165.

MRI data, displacement fields and strain fields may be obtained for use in validating computer models by email request to baylyp@seas.wustl.edu.

REFERENCES

Axel, L. & Dougherty, L. 1989 Heart wall motion: improved method of spatial modulation of magnetization for MR imaging. *Radiology* **172**, 349–350.

Bayly, P. V., Cohen, T. S., Leister, E. P., Ajo, D., Leuthardt, E. C. & Genin, G. M. 2005 Deformation of the human brain induced by mild acceleration. *J. Neurotrauma* **22**, 845–856. (doi:10.1089/neu.2005.22.845)

Cloots, R. J., Gervaise, H. M., Van Dommelen, J. A. & Geers, M. G. 2008 Biomechanics of traumatic brain injury: influences of the morphologic heterogeneities of the cerebral cortex. *Ann. Biomed. Eng.* **36**, 1203–1215. (doi:10.1007/s10439-008-9510-3)

Gosch, H. H., Gooding, E. & Schneider, R. C. 1969 Distortion and displacement of the brain in experimental head injuries. *Surg. Forum* **20**, 425–426.

Hardy, W. N., Foster, C. D., Mason, M. J., Yang, K. H., King, A. I. & Tashman, S. 2001 Investigation of head injury mechanisms using neutral density technology and high-speed biplanar X-ray. *Stapp Car Crash J.* **45**, 337–368.

Hodgson, V. R., Gurdjian, E. S. & Thomas, L. M. 1966 Experimental skull deformation and brain displacement demonstrated by flash X-ray technique. *J. Neurosurg.* **25**, 549–552. (doi:10.3171/jns.1966.25.5.0549)

Ivancevic, V. G. 2009 New mechanics of traumatic brain injury. *Cogn. Neurodyn.* **3**, 281–293. (doi:10.1007/s11571-008-9070-0)

Ji, S. B. & Margulies, S. S. 2007 *In vivo* pons motion within the skull. *J. Biomech.* **40**, 92–99. (doi:10.1016/j.jbiomech.2005.11.009)

Kimpara, H., Nakahira, Y., Iwamoto, M., Miki, K., Ichihara, K., Kawano, S. & Taguchi, T. 2006 Investigation of anteroposterior head–neck responses during severe frontal impacts using a brain–spinal cord complex FE model. *Stapp Car Crash J.* **50**, 509–544.

Kleiven, S. & Hardy, W. 2002 Correlation of an FE model of the human head with local brain motion—consequences for injury prediction. In *Proc. 46th Stapp Car Crash Conf., Pante Vedra Beach, FL.* SAE paper, 2002-22-0007, pp. 123–144.

Ommaya, A. K., Boretos, J. W. & Beile, E. E. 1969 The Lexan calvarium: an improved method for direct observation of the brain. *J. Neurosurg.* **30**, 25–29.

Osman, N. F., Mcveigh, E. R. & Prince, J. L. 2000 Imaging heart motion using harmonic phase MRI. *IEEE Trans. Med. Imaging* **19**, 186–202. (doi:10.1109/42.845177)

Pudenz, R. H. & Shelden, C. H. 1946 The Lucite Calvarium—a method for direct observation of the brain. *J. Neurosurg.* **3**, 487–505. (doi:10.3171/jns.1946.3.6.0487)

Raul, J. S., Deck, C., Willinger, R. & Ludes, B. 2008 Finite-element models of the human head and their applications in forensic practice. *Int. J. Legal Med.* **122**, 359–366. (doi:10.1007/s00414-008-0248-0)

Sabet, A. A., Christoforou, E., Zatlin, B., Genin, G. M. & Bayly, P. V. 2008 Deformation of the human brain induced by mild angular head acceleration. *J. Biomech.* **41**, 307–315. (doi:10.1016/j.jbiomech.2007.09.016)

Shatsky, S. A., Alter III, W. A., Evans, D. E., Armbrustmacher, V. W., Clark, G. & Earle, K. M. 1974 Traumatic distortions of the primate head and chest: correlation of biomechanical, radiological and pathological data. In *Proc. 18th Stapp Car Crash Conf., Ann Arbor, MI.* pp. 351–381.

Shelden, C. H., Pudenz, R. H., Restarski, J. S. & Craig, W. M. 1944 The lucite calvarium—a method for direct observation of the brain. *J. Neurosurg.* **1**, 67–75. (doi:10.3171/jns.1944.1.1.0067)

Smith, D. H. & Meaney, D. F. 2000 Axonal damage in traumatic brain injury. *Neuroscientist* **6**, 483–495. (doi:10.1177/107385840000600611)

Stalnaker, R. L., Melvin, J. W., Nusholtz, G. S., Alem, N. M. & Benson, J. B. 1977. Head Impact Response. *Proceedings of the 21st Stapp Car Crash Conference*, pp. 305–335.

Zhang, L., Yang, K. H., Dwarampudi, R., Omori, K., Li, T., Chang, K., Hardy, W. N., Khalil, T. B. & King, A. I. 2001 Recent advances in brain injury research: a new human head model development and validation. *Stapp Car Crash J.* **45**, 369–394.

Zhang, L., Yang, K. H. & King, A. I. 2004 A proposed injury threshold for mild traumatic brain injury. *J. Biomech. Eng.* **126**, 226–236. (doi:10.1115/1.1691446)

Zou, H., Schmiedeler, J. P. & Hardy, W. N. 2007*a* Separating brain motion into rigid body displacement and deformation under low-severity impacts. *J. Biomech.* **40**, 1183–1191. (doi:10.1016/j.jbiomech.2006.06.018)

Zou, H., Kleiven, S. & Schmiedeler, J. P. 2007*b* The effect of brain mass and moment of inertia on relative brain–skull displacement during low-severity impacts. *Int. J. Crashworthiness* **12**, 341–353.